Total Surface Area Estimates for Individual Ice Particles and Particle Populations

C. G. SCHMITT AND A. J. HEYMSFIELD

National Center for Atmospheric Research, Boulder, Colorado

(Manuscript received 23 December 2003, in final form 10 September 2004)

ABSTRACT

Representations for the surface area of ice particles in terms of the projected area have been developed using two different methods. The first method uses ice particles that are imaged in situ and geometric calculations that are based on the outline of the two-dimensional image of the particle. The second method uses computer-generated ice particle shapes and calculates the total surface area analytically. The results of the second method compare reasonably well with the results of the first method. Surface area estimates for individual particles were combined with particle size distribution and projected area measurements from the Cirrus Regional Study of Tropical Anvils and Cirrus Layers (CRYSTAL)–Florida Area Cirrus Experiment (FACE) field project to give total surface area estimates for observed ice particle populations. Population surface area estimates were also made from balloon-borne replicator data collected during the First International Satellite Cloud Climatology Project (ISCCP) Regional Experiment, phase II (FIRE-II). A relationship between the particle population surface area and projected area (cloud extinction) has been derived. The total particle surface area for particle populations is estimated to be between 8 and 10 times the projected area or between 4 and 5 times the extinction and has a small dependence on the properties of the particle size distribution for particles observed in random orientations.

1. Introduction

Accurate estimates of ice particle surface areas for individual particles or populations are necessary for a wide range of atmospheric problems. Ice particles observed in clouds are dominated by complex shapes (Korolev and Sussman 2000); therefore, the surface area of individual particles is not easily calculated. This paper addresses the calculation of the surface area of complex ice particle shapes.

Studies of the uptake of pollutants by ice particles require accurate particle population surface area (A_{sp}) estimates (Lawrence and Crutzen 1998). Salomon et al. (1997) estimated the individual particle surface area (A_{si}) using an empirical relationship originally derived for sulfate aerosols. These estimates were used to develop zonally and seasonally averaged A_{sp} estimates for cirrus clouds. These averaged estimates are used by Feigl et al. (1999) and are compared to direct measurements using a Multiangle Aerosol Spectrometer (MASP) particle probe, yet Feigl et al. (1999) do not detail how estimates were made from the particle measurements. Meier and Hendricks (2002) calculated particle A_{si} using hexagonal ice particle shapes, implying that a factor of 4 times the projected area (A_{pi}) was used to calculate surface area, which is reasonable for randomly oriented particles without concavities (Vouk 1948).

The total surface area of ice particles is necessary for the calculation of the equivalent sphere size for the equivalent sphere radiation approximation put forth by Grenfell and Warren (1999). In this theory, equivalent spheres of equal total surface area and equal total volume are used to represent the scattering properties of ice crystals or ice crystal populations (Neshyba et al. 2003). The total particle surface area, including the surface area of concavities, is used, meaning that the factor of 4 times the surface area put forth by Vouk (1948) is not directly applicable. Total particle surface area estimates are key to calculating the correct equivalent sphere sizes because the theory relies both on the extinction of the sphere population and the scattering properties of the spheres.

This paper seeks to provide reliable estimates of A_{si} as well as A_{sp}. Section 2 briefly describes the observational cloud particle data used in this study. In section 3 the techniques used for estimating A_{si} are discussed and use guidelines are presented. In section 4 the results are used to parameterize optical depth to A_{sp} relationships for aircraft measurements and balloon-borne replicator data. In section 5 the work is summarized.

Corresponding author address: Carl Schmitt, 3450 Mitchell Lane, P.O. Box 3000, Boulder, CO 80301.
E-mail: schmittc@ucar.edu

2. Overview of ice particle data

In situ measurements used in this study were collected aboard the University of North Dakota Citation aircraft during the Cirrus Regional Study of Tropical Anvils and Cirrus Layers (CRYSTAL)–Florida Area Cirrus Experiment (FACE) field project in southern Florida in July 2002. The ice clouds that were observed were convectively generated ice or anvil cirrus clouds at temperatures from 0° to −70°C.

Detailed particle images were recorded with the Stratton Park Engineering Company (SPEC, Inc.) Cloud Particle Imager (CPI) probe. The CPI images have 2.3-μm pixels rendering a roughly 10-μm resolution. The outline of the high-resolution images was used to estimate the surface roughness of the ice particles. Size distribution data from the CPI was not used because of the limited sample volume as well as sample volume uncertainties that were caused by the triggered imaging system.

For particle size distribution measurements above 45 μm in maximum dimension (D), the Particle Measuring Systems (PMS), Inc., two-dimensional cloud probe (2DC) and the SPEC, Inc., High Volume Precipitation Sampler (HVPS) cloud probe were used. The techniques used to calculate raw size distributions from the 2DC and HVPS are given in Heymsfield et al. (2002a). The PMS Forward Scattering Spectrometer Probe (FSSP) was used for the measurement of particles smaller than 45 μm. The FSSP measurements may be overestimated because of the breakup of large ice particles on the inlet of the probe (Field et al. 2003), as well as ice particle sizing uncertainties. The effects that these uncertainties have on the results of this work are investigated later. Composite size distributions were obtained by merging the spectra obtained from the FSSP, 2DC, and HVPS probes. The particle size distributions from the 2DC and HVPS composite size distributions were fitted to a gamma curve of the form $N = N_o D^{\mu} e^{-\lambda D}$ where N_o is the intercept, λ is the slope, and μ is the dispersion. The moment-matching method used the first, second, and sixth moments to provide the best fit over the size distributions, as described in Heymsfield et al. (2002a).

In situ measurements were also obtained with the National Center for Atmospheric Research (NCAR) balloon-borne replicator. This instrument collects data in the 10–500 μm or greater size range. Instrument collection efficiency for small particles is accounted for. This instrument sampled cirrus clouds (temperatures from −20° to −65°C) over Kansas on 3 days during the First International Satellite Cloud Climatology Project (ISCCP) Regional Experiment, phase II (FIRE-II) in November and December of 1991. Details of the analysis of the replicator data can be seen in Miloshevich and Heymsfield (1997). A dataset for each of the three cases consisted of the characteristics of all of the imaged ice particles, including particle area and maximum dimension.

3. Surface area using high-resolution particle imagery

a. Theory for surface area estimates from 2D particle images

The estimation of a particle's surface area from a 2D image, obtained by an aircraft imaging probe, begins with the premise that to the first order the total surface area of a sphere can be calculated from its 2D image. One can calculate the length of the perimeter, then calculate the radius, and then calculate the surface area using the radius. The authors propose that for irregular shapes the same methods can be used to obtain an estimate of the total surface area.

The surface area calculation method for a complex ice particle image first considers the fact that the average surface area of a randomly oriented convex particle, as well as that of a sphere, is 4 times the average projected area (Vouk 1948),

$$A_{si} = \overline{A_{pi}}4, \tag{1}$$

where $\overline{A_{pi}}$ is the average projected area and A_{si} is the surface area of the individual particle. Most of the particles that are observed in the atmosphere have concavities, meaning that Eq. (1) underestimates the surface area for most atmospheric ice particles. Equation (1) can be broken down into a more useful form that still holds true for spheres using $\overline{A_{pi}} = \pi r^2$. Because the perimeter of the particle $p = 2\pi r$, p can be substituted in, giving $\overline{A_{pi}} = rp/2$. Substituting this into Eq. (1) gives

$$A_{si} = 2rp, \tag{2}$$

where r is the radius and p is the perimeter (or outline) of the projected 2D particle. Equation (2) assumes that $\overline{A_{pi}}$ is being replaced by A_{pi}, which is the projected area of a randomly oriented particle. This will result in errors when the surface area of individual particles is estimated, but it is thought that the result is useful if results from many particles are averaged together. By breaking the perimeter up into small segments and summing, Eq. (2) can be transformed, without loss for spheres, into Eq. (3):

$$A_{si} = 2\sum_{i=0}^{i_{max}} r_i p_i, \tag{3}$$

where i is the number of points on the edge, r_i is the radius to the ith outline point from the center of the particle, and p_i is the length calculated for the ith outline point. The coordinates of the center of the particle in the x–y plane are calculated by averaging the x and y components of all of the pixels that make up the particle image. The radius unit for each outline point (r_i) is

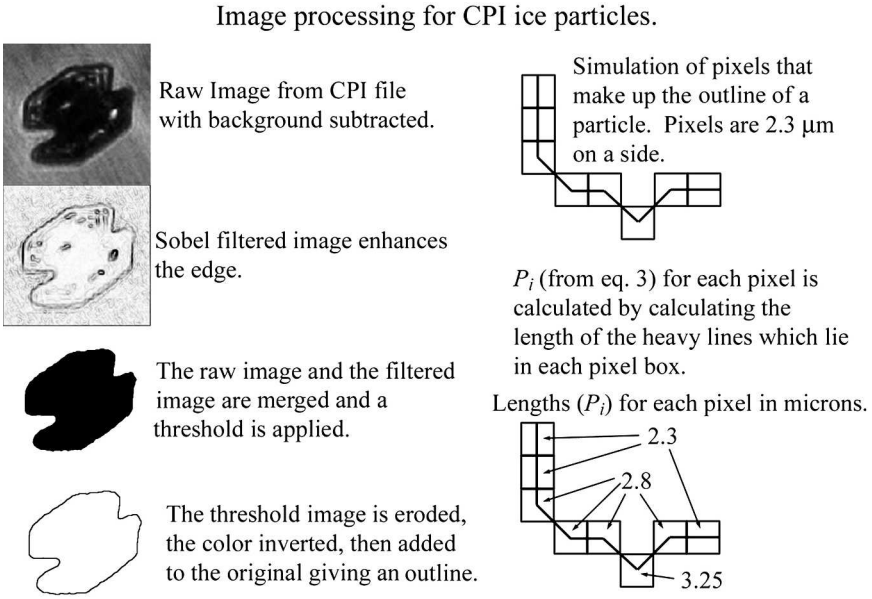

FIG. 1. Diagram showing how the CPI particle imagery data are processed for this study: (left) how the particle edge is determined and (right) how the value of P_i is found for each point on the outline.

the distance from the center of the particle image to the *i*th outline point. Equation (3) is valid for spheres. The authors believe that it can be used to provide an estimate of the total surface area of irregular particles as well.

b. Applying theory to particle images

A total of 12 000 particles imaged by the CPI probe during CRYSTAL-FACE, representing approximately 10% of the Citation CPI data, were analyzed in developing surface area estimates. Particles smaller than 150 μm were not used because the pixel size adversely affects the perimeter calculation for these small particles. Particles from time periods that were chosen randomly gave a dataset from a variety of temperatures, pressures, and cloud types. The sample was limited because of the highly intensive nature of the computer calculations. The results were very consistent. When the dataset was broken up into subsets, the resulting fit lines were nearly indistinguishable from each other when plotted together.

To apply Eq. (3) to CPI data, it was necessary to define the 2D particle outline accurately. The outline of each particle was graphically determined with specially developed image processing software. The particle image was first simplified by making it into a black and white binary image where pixels above a threshold were changed to ones and all other pixels were changed to zeros. This was accomplished by combining the image with an image created using a basic Sobel edge-detecting filter. The Sobel edge detector uses a pair of masks, which are much smaller than the image, to estimate the local gradient in pixel values for each point in the image (Pratt 1978). The combined image with enhanced edges was then changed into a binary image. The threshold was determined by averaging the pixel values for the entire image and applying a factor based on the data quality. Lower-valued pixels within the particle were also given a value of 1 so that the particles were filled. The Sobel filter also was used to determine whether the particles were in focus. Out-of-focus particles were not processed. Accepted particles corresponded to particles that were assigned a focus value of about 40% or better by SPEC, Inc.,'s CPIview software. An erode function was used to remove one pixel from the outer edge of the black and white particle. The eroded image was subtracted from the original image, leaving the outermost pixels of the particle. The technique, similar to the technique used by Korolev and Sussman (2000), is shown graphically in Fig. 1. For each outlined pixel, a perimeter segment length [p_i in Eq. (3)] was calculated based on the pixel's orientation to neighboring outline pixels. A line was drawn from the center point of the outline pixel to the center point of each neighboring outline pixel. The length assigned the pixel is the sum of the lengths of the lines within the square. This technique is also shown graphically in Fig. 1. The distance from each point on the edge to the center of the particle is calculated [r_i in Eq. (3)].

Given a value of r_i and P_i for each edge pixel, Eq. (3) was applied to estimate the total surface area of the 12 000 CPI particles, and the ratio of the estimated A_{si} to A_{pi} was calculated. The results show a strong correlation to the area ratio (A_r) of the particle. The area

ratio of the particle is the ratio of the A_{pi} and the area of the smallest circle that can completely enclose the particle. For the 12 000 particles that were analyzed, the ratio of the A_{si}/A_{pi} has been plotted versus A_r of the particles in Fig. 2. The 10th- and 90th-percentile values are also plotted to give an idea of the potential error. Note that high A_r particles (which might be thought of as spherical frozen droplets) have A_{si}/A_{pi} ratios of about 4.0, as would be expected for spheres. A fit to the median values for the data in 0.05 steps of A_r is given in Eq. (4):

$$A_{si}/A_{pi} = 4.0A_r^{-0.6}. \quad (4)$$

c. Surface area from theoretically generated particles

Computer-simulated column-, plate-, and bullet rosette–shaped ice crystals with different aspect ratios and degrees of hollowness were used. Computer-simulated hollow columns have six-sided pyramids of ice absent at both ends. Hollow rosettes have these hollows at their outer ends. These particles grow in regions of high supersaturation (Bailey and Hallett 2004). Examples of computer-generated hollow columns are among the particles that are shown in Fig. 3. Bullet rosette ice crystals are often the predominant habit in midlatitude cirrus (Heymsfield et al. 2002b), while plates and columns are often seen in combination with irregular particles. Most observed ice crystals are irregular (Korolev and Sussman 2000) and do not appear to be similar to these theoretically generated ice particles. The A_{si} of the individual theoretical particles was determined analytically. Several thousand random orientations of each particle type have been taken in order to identify the area ratio range for the particles. Figure 3 shows the A_{si}/A_{pi} ratios that are plotted versus A_r for the three modeled crystal types, as well as images of some of the modeled ice particles. For plate-shaped crystals, particles with diameter-to-thickness ratios from 1.5 to 10.0 were used. For column-shaped crystals diameter-to-length ratios from 0.6 to 0.1 were used, as well as a range of hollowness factors. For bullet rosettes, rosettes with six bullets with bullet length–to-diameter ratios of 5.0 were used. This bullet rosette formation is representative of the bullet rosettes that are typically observed in midlatitude cirrus (Heymsfield et al. 2002b). Fits of A_{si}/A_{pi} for all orientations of each particle type, as well as fits for the maximum projected area for each particle type, have been determined and are on the respective plots. The maximum projected area fit is useful for determining A_{si}/A_{pi} for oriented particles. Table 1 summarizes the fit data from the theoretical particles. Results for more complicated particle shapes (i.e., capped columns, dendrites, etc.) were not calculated because particles of those types are rarely uniform throughout a cloud and, therefore, the authors believe that the results would not be useful.

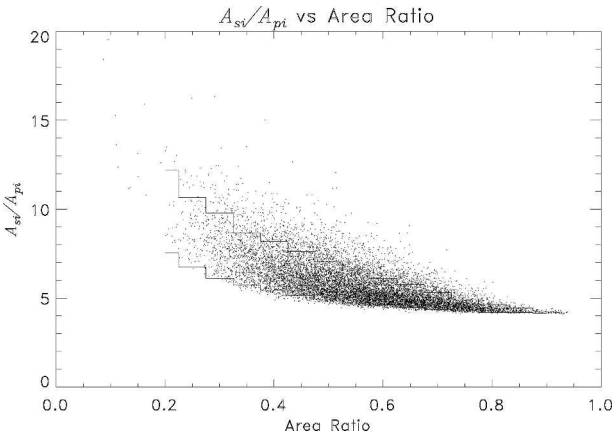

FIG. 2. The ratio A_{si}/A_{pi} for 12 000 CPI particles plotted vs the particle A_r. The solid lines show the 10th- and 90th-percentile values for each range of A_r values.

d. Estimates to account for expected surface roughness

The theoretical particles that were used for the results in Table 1 were assumed to have smooth surfaces, which is unlikely for most particles. The Table 1 results can be considered a lower-bound value for the A_{si}/A_{pi} ratio. The authors believe that a reasonable upper bound for the A_{si}/A_{pi} ratio can be estimated by assuming that the particle surface is covered with hemispheric protrusions. This can be thought of as the particle surface being coated with frozen rime droplets and taking the shape of hemispheres. If the surface were coated with tightly packed hemispheres the surface area would be increased by a factor of 1.78. Table 2 summarizes the recommended surface area enhancements for the different cloud types. This surface area enhancement can also be applied to the equation for irregular particles to account for surface markings that are too small to be seen by the CPI. Because crystals with either very smooth or very rough surfaces may dominate some cloud types, a useful A_{si}/A_{pi} relationship should be adjusted, based on cloud type, for the best results. Equation (5) shows good compromise values if cloud crystal type and complexity is unknown:

$$A_{si}/A_{pi} = 5.6A_r^{-0.6}. \quad (5)$$

Equation (5) will be used for the remainder of this study.

For the particles shown in Fig. 3, the A_{si} has been calculated analytically, as well as with the technique using Eq. (3). The ratio of A_{si} versus the Eq. (3)–estimated A_{si} is plotted in Fig. 4. The results show that the technique that is for used for irregular particles overestimates the surface area of the pristine particles by a factor of 1.88, on average. While this discrepancy may seem excessive, one must consider the simplicity of the particles modeled for Fig. 3 in comparison with the

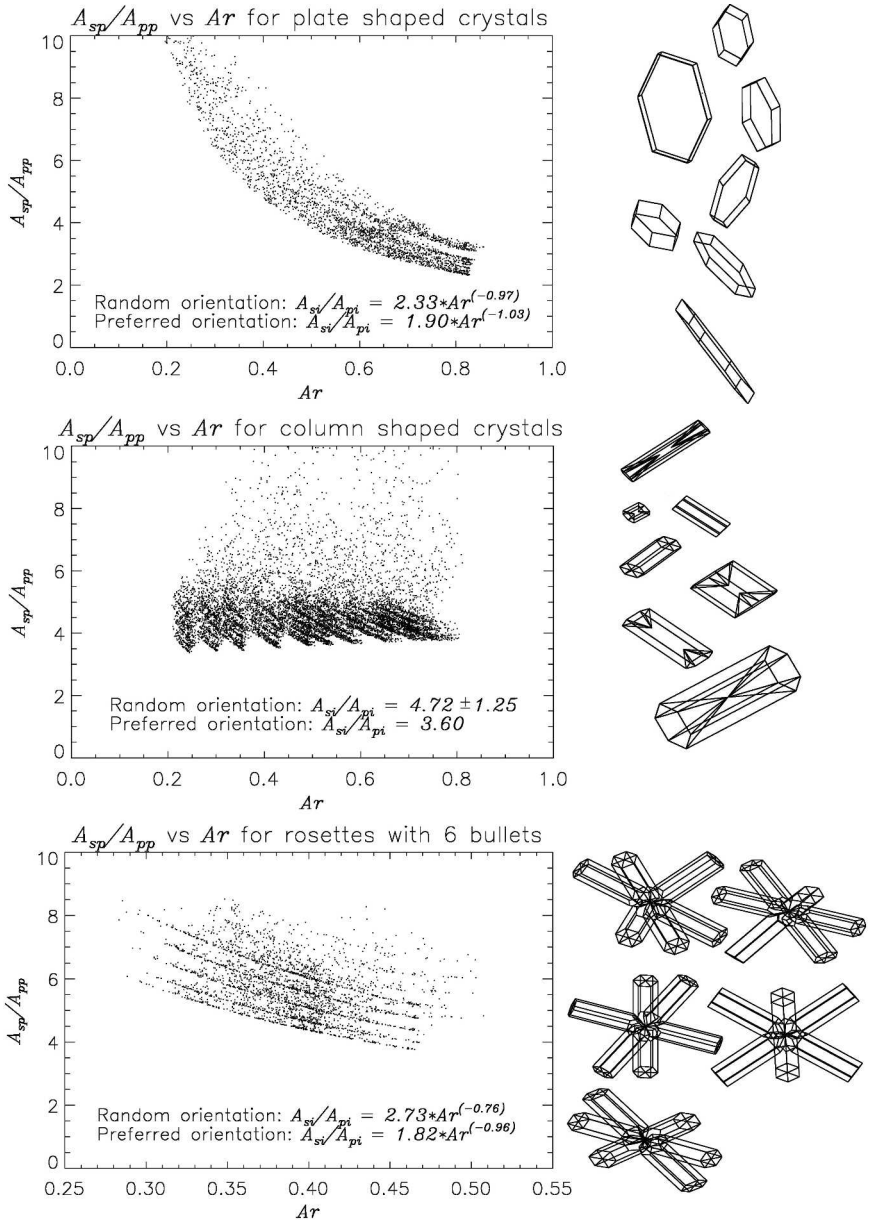

FIG. 3. The ratio A_{si}/A_{pi} for various computer-generated ice particles plotted vs the A_r for random orientations of the particles. Examples of the computer-generated particle types are also shown.

extremely irregular particles shown in Fig. 4. While it is not possible to accurately know the A_{si} of irregular particles, the authors believe that the factor of 1.88 is reasonable, given the range of natural variability.

4. Relating extinction to total particle surface area

A useful conclusion to this work would be the development of a reliable A_{sp} to the cloud extinction relationship. This would facilitate estimates of A_{sp} from extinction measurements of optically thin clouds with lidar. The work leading to Eq. (5) assumes that the imaged particles are randomly oriented when they are imaged. The image projections of the 2DC-imaged particles have been investigated to estimate the validity of this assumption. Data collected by the 2DC while it was mounted in two perpendicular orientations were used to evaluate whether the particle images are biased by probe orientation. The difference in the A_r that were measured in the two 2DC probe orientations was negligible, indicating that the A_r values measured by the 2DC are representative of the particles. While this con-

TABLE 1. Fits for A_{si}/A_{pi} of computer-generated ice particles.

Particle type	Random orientation	Preferred orientation
Plates	$A_{si}/A_{pi} = 2.33A_r^{-0.97}$	$A_{si}/A_{pi} = 1.90A_r^{-1.03}$
Columns	$A_{si}/A_{pi} = 4.72 \pm 1.25$	$A_{si}/A_{pi} = 3.60$
Bullet rosettes	$A_{si}/A_{pi} = 2.73A_r^{-0.76}$	$A_{si}/A_{pi} = 1.82A_r^{-0.96}$

clusion does not assure that the particles are randomly oriented, the authors feel that it justifies the use of Eq. (5).

a. CRYSTAL–FACE data

For the CRYSTAL–FACE particle size distribution measurements, A_r was derived from an analysis of the data from the 2DC and HVPS, and an average value was obtained for each of the 33 sized bins that were used to represent the data throughout the flights. The A_r for FSSP-sized particles was assumed to be 0.80, which is reasonable for small frozen droplets that have undergone some growth. Variations in this value did not affect the final results significantly. The FSSP concentrations are likely to be overestimated, but sizing errors could produce unknown effects. Increase or decrease the FSSP particle concentration by a factor of 10, which results in a 10% change in the A_{sp}/A_{pp} results, addressed the potential sizing and concentration errors. Particle size distribution data from the FSSP, 2DC, and HVPS were averaged over 5-s time periods throughout the CRYSTAL–FACE dataset. Data from 9, 11, 16, 18, 21, 23, 25, 26, 28, and 29 July were used in this analysis, resulting in 11 385 usable 5-s time periods. The ratio of A_{sp}/A_{pp} was calculated for the size distributions from particle size distributions and A_r data. Figure 5 shows A_{sp}/A_{pp} plotted versus the particle size distribution spectral slope λ from the gamma fit to the size distribution. Equation (6) shows that the curve was fit to the median values taken at 5-cm^{-1} increments in λ:

$$A_{sp}/A_{pp} = 9.8\lambda^{-0.03}. \quad (6)$$

TABLE 2. Suggested equation parameters for estimating A_{si}/A_{pi} for irregular particles from the particle A_r. Equation is of the form $A_{si}/A_{pi} = bA_r^{-0.6}$.

Cloud type	b*	Cloud and cloud particle properties
Vapor-grown cloud particles	4.0	Pristine particles; clouds generally have halos.
General case	5.6	Estimate if particle properties are unknown.
Rimed irregular particles	7.3	Convective clouds; no halos are observed.

* The values for b were estimated by assuming smooth particle surfaces (vapor-grown cloud particles), or rough particle surfaces (heavily rimed irregular particles). If surface properties are unknown the value of b can be estimated as halfway between the other two cases.

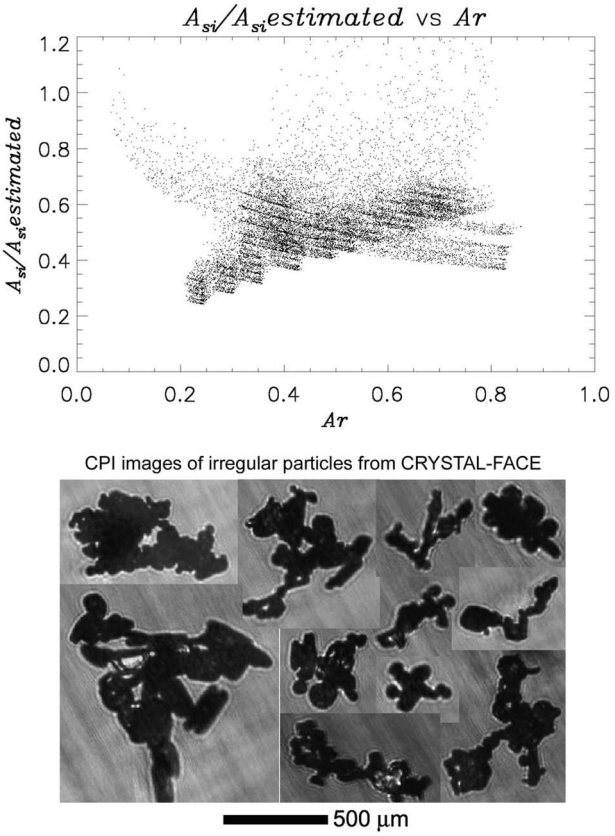

FIG. 4. (top) Ratio of the actual A_{si} over A_{si} estimated using Eq. (3) plotted vs A_r for the particles simulated in Fig. 3. (bottom) Highly irregular ice particles imaged by the CPI during CRYSTAL–FACE.

Figure 5 shows that for the particle size distributions observed during the CRYSTAL–FACE field project, the A_{sp}/A_{pp} was rarely less than 8 or greater than 10. Typical λ values for convective clouds can be found in Heymsfield et al. (2002a). The geometric optics ap-

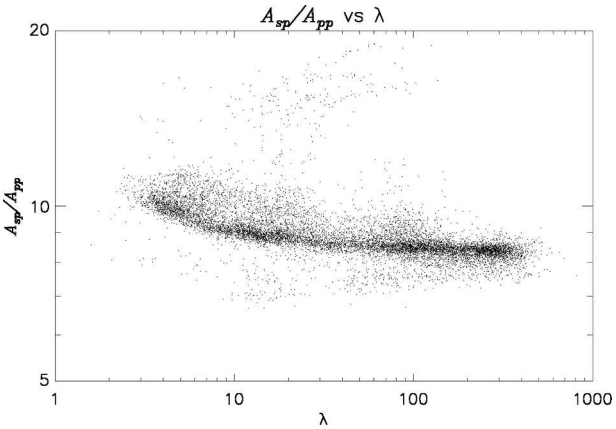

FIG. 5. The ratio A_{sp}/A_{pp} for size distributions plotted vs the λ value from the gamma fit to the particle size distribution from the CRYSTAL–FACE field project.

TABLE 3. Suggested equations for total particle surface area based on cloud type. If extinction Ext is in units of cm^{-1}, then A_{sp} will be in units of cm^2 cm^{-3}.

Cloud type	Surface area estimate
Vapor-grown cloud particles	$A_{sp} = \text{Ext} \times 3.5\lambda^{-0.030}$
General case	$A_{sp} = \text{Ext} \times 4.9\lambda^{-0.030}$
Heavily rimed irregular particles	$A_{sp} = \text{Ext} \times 6.4\lambda^{-0.030}$

proximation says that extinction is 2 times the projected area for the particle population (Mishchenko et al. 2002). Based on the results summarized in Table 1, an estimate can be made to modify the calculations based on observations of randomly oriented particles to values for preferred orientations. Table 3 summarizes suggested values for converting cloud extinction into estimates of A_{sp} based on cloud type.

b. Replicator data

A balloon-borne replicator was used to sample cirrus clouds during the FIRE-II field campaign. The cirrus clouds generally consisted of small particles, and the gamma fits obtained for all of the collected particles resulted in high values of λ. For each altitude, the A_{sp} was calculated using Eq. (5) and the A_{pp} was summed, giving an A_{sp}/A_{pp} relationship for the FIRE-II data. These results were generated from individual particles, not from derived size distributions and averaged area ratio values. Figure 6 shows A_{sp}/A_{pp} by altitude for three ascents during the Fire-II research project. The higher values calculated for the 25 November 1991 data are likely due to the high concentration of columns in replicator data at those altitudes. Columns have low A_r values, which lead to a higher A_{sp}/A_{pp} ratio when using Eq. (5). Figure 7 shows the λ versus the A_{sp}/A_{pp} ratio for the replicator data;

$$A_{sp}/A_{pp} = 8.9\lambda^{-0.03} \quad (7)$$

shows the A_{sp}/A_{pp} versus λ relationship for the FIRE-II data. The similarity between Figs. 5 and 7 [as well as Eqs. (6) and (7)] shows that it is reasonable to calculate surface area from particle size distributions and averaged values of A_r.

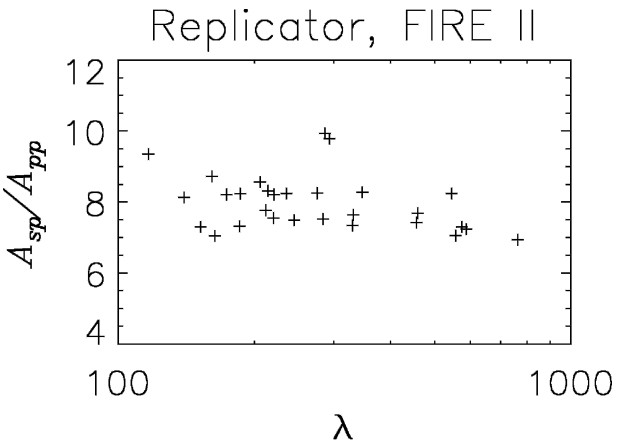

FIG. 7. The ratio A_{sp}/A_{pp} for size distributions plotted vs the λ value from the gamma fit to the particle size distribution from the replicator.

5. Summary

The total surface area of ice particles has been estimated using ice particles that are imaged in situ as well as computer-generated ice particles. The total particle surface area estimates were found to agree well by using both techniques, and a parameterization relating particle-projected area and particle area ratio has been developed to predict the surface area. This study examines variations from the expected cloud particle surface roughness, which produced an uncertainty of plus or minus a factor of 1.5. While it is impossible to know the exact surface area of irregular ice particles, it is believed that the estimates that are presented here are more realistic. This technique is based on observed properties of ice particles (their outline), rather than parameterizations based on sulfate particles or the surface

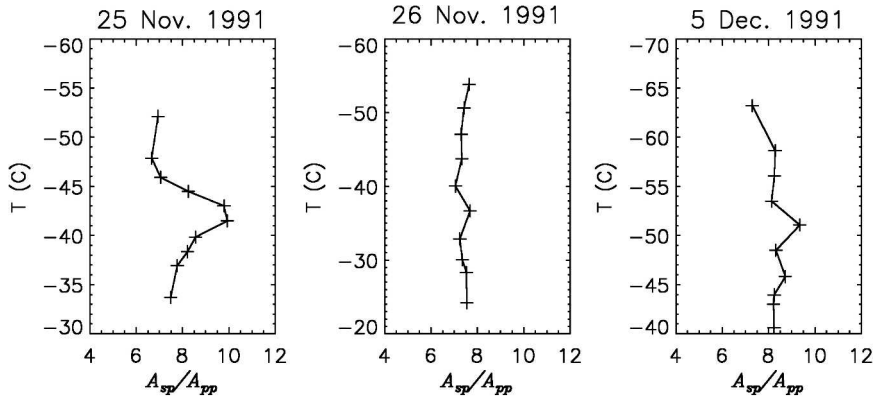

FIG. 6. The ratio A_{sp}/A_{pp} for 3 days of replicator data plotted by temperature.

area of spheres with the same maximum dimension as the ice particles.

The surface area parameterization was applied to particle size distributions that were observed during the CRYSTAL–FACE field project. A parameterization was developed to relate visible light extinction to the total particle surface area for a particle population. For confirmation, the surface area to projected area parameterization was also applied to balloon-borne replicator data, where the surface area was calculated for particles on an individual basis and the projected area was summed for observed particle populations. The results were in good agreement with the values calculated for the CRYSTAL–FACE data, showing that these parameterizations are useful for many different cloud types and that the data averaging does not significantly affect the results.

A reliable estimate of the total particle surface area of a population of ice particles can now be made from extinction measurements. This parameterization should be useful for calculating deposition rates of atmospheric compounds on ice crystals, for particle growth estimates, and for the calculation of the radiative properties of ice clouds using equal surface area and volume equivalent spheres.

Acknowledgments. This research was supported by the NASA CRYSTAL program through NASA-NSF Agreement W-10, 024, Don Anderson being program manager. The authors are indebted to the crew of the UND Citation aircraft.

REFERENCES

Bailey, M., and J. Hallett, 2004: Growth rates and habits of ice crystals between −20° and −70°C. *J. Atmos. Sci.,* **61,** 514–544.

Feigl, C., H. Schlager, H. Ziereis, J. Curtius, F. Arnold, and C. Schiller, 1999: Observations of NO_y uptake by particles in the Arctic tropopause region at low temperatures. *Geophys. Res. Lett.,* **26,** 2215–2218.

Field, P., R. R. Wood, P. R. A. Brown, P. H. Kaye, E. Hirst, R. Greenaway, and J. A. Smith, 2003: Particle interarrival times measured with a Fast FSSP. *J. Atmos. Oceanic Technol.,* **20,** 249–261.

Grenfell, T. C., and S. G. Warren, 1999: Representation of nonspherical ice particles by a collection of independent spheres for scattering and absorption of radiation. *J. Geophys. Res.,* **104,** 31 697–31 709.

Heymsfield, A. J., A. Bansemer, P. R. Field, S. L. Durden, J. L. Stith, J. E. Dye, W. Hall, and C. A. Grainger, 2002a: Observations and parameterizations of particle size distributions in deep tropical cirrus and stratiform precipitating clouds: Results from in situ observations in TRMM field campaigns. *J. Atmos. Sci.,* **59,** 3457–3491.

——, S. Lewis, A. Bansemer, J. Iaquinta, L. Milosovich, M. Kajikawa, C. Twohy, and M. Poellot, 2002b: A general approach for deriving the properties of cirrus and stratiform ice cloud particles. *J. Atmos. Sci.,* **59,** 3–29.

Korolev, A., and B. Sussman, 2000: A technique for habit classification of cloud particles. *J. Atmos. Oceanic Technol.,* **17,** 1048–1057.

Lawrence, M. G., and P. J. Crutzen, 1998: The impact of cloud particle gravitational settling on soluble trace gas distributions. *Tellus,* **50B,** 263–289.

Meier, A., and J. Hendricks, 2002: Model studies on the sensitivity of upper tropospheric chemistry to heterogeneous uptake of HNO_3 on cirrus ice particles. *J. Geophys. Res.,* **107**, 4696, doi:10.1029/2001JD000735.

Miloshevich, L. M., and A. J. Heymsfield, 1997: A balloon-borne continuous cloud particle replicator for measuring vertical profiles of cloud microphysical properties: Instrument design, performance, and collection efficiency analysis. *J. Atmos. Oceanic Technol.,* **14,** 753–768.

Mishchenko, M. I., L. D. Travis, and A. A. Lacis, 2002: *Scattering, Absorption, and Emission of Light by Small Particles.* Cambridge University Press, 445 pp.

Neshyba, S. P., T. C. Grenfell, and S. G. Warren, 2003: Representation of a nonspherical ice particle by a collection of independent spheres for scattering and absorption of radiation, II. *J. Geophys. Res.,* **108**, 4448, doi:10.1029/2002JD003302.

Pratt, W. K., 1978: *Digital Image Processing.* John Wiley and Sons, 750 pp.

Salomon, S., S. Borrmann, R. R. Garcia, R. Portmann, L. Thomason, L. R. Poole, D. Winker, and M. P. McCormick, 1997: Heterogeneous chlorine chemistry in the tropopause region. *J. Geophys. Res.,* **102,** 21 411–21 429.

Vouk, V., 1948: Projected area of convex bodies. *Nature,* **162,** 330–331.